TECHNICAL PAPER

CrossMark

Numerical and experimental investigations on the performance of a serpentine microchannel with semicircular obstacles

Sandeep Sitaram Wangikar[1,2] · Promod Kumar Patowari[1] · Rahul Dev Misra[1]

Abstract

This paper focuses on computational and experimental analysis of a simple serpentine microchannel without obstacles and serpentine microchannel with semicircular obstacles of different sizes. The work has been performed in three phases-computational analysis, experimentation and flow physics study. The 3D models of a simple serpentine microchannel (without obstacles) and serpentine microchannels with semicircular obstacles (with radius as 50, 100, 150 and 200 μm) have been developed using COMSOL Multiphysics software. The effect of obstacle size on pressure drop and mixing length for achieving index 1 has been analyzed. A simple serpentine qmicrochannel and a serpentine microchannel with 150 μm radius semicircular obstacles have been fabricated with polydimethylsiloxane using soft lithography process. The experimental analysis for pressure drop as well as mixing index has been performed. A good agreement has been observed between experimental and computational results. The validated computational model is then used to study the mixing index for the same microchannels for different flow conditions, i.e. for different Reynolds numbers. The mixing lengths are observed to be lesser for Re 0.28 and 30. Further, the effect of diffusion and generation of secondary flow due to advection on mixing length for the considered Reynolds numbers are analyzed through the flow physics study.

1 Introduction

The microfluidic systems are the most growing technology, and the microfluidics study is significant for implementing Lab on chips. The Lab on chip systems which are moreover recognized as micro total analysis systems (μTAS) that can execute maximum stages of chemical and biological processes (Lim et al. 2010). The role of microfluidic chip is noteworthy in the field of biomedicine and biochemistry. The performance of many microfluidic devices is dependent on a fast and efficient mixing of the species which is incorporated through a micromixer. Thus, a micromixer is the prominent component of a microfluidic system. The micromixers is classified into two categories as—active micromixer and passive micromixer (Capretto et al. 2011). An external energy source is required in active micromixers for the mixing enhancement, like magneto

hydrodynamics, acoustic pressure, etc. Active micromixer generally provides correct mixing, but their fabrication is cost intensive and integration with different devices is difficult. For this reason, passive micromixers are favored in number of situations. In the passive micromixers, different geometric shapes and/or fluid characteristics are effectively used. The mixing between different species inside the microchannel might not be superior because of laminar flow and the mixing depends only upon the mass diffusion. As a way to enhance the mixing in microchannels, various methods have been developed in recent years (Lee et al. 2016). There are different approaches to enhance mixing characteristics of the microchannels using the various shapes of microchannels or by putting obstacles in the microchannels. Thus, selecting the microchannel configuration is a notable concern for efficient mixing. Some of the relevant studies in the recent past are presented below.

Sahu et al. (2012, 2013) have analyzed mixing numerically as well as experimentally for a rectangular microchannel with Y-type inlet and passive micromixer with symmetric and staggered obstructions. They reported that there is significant effect of aspect ratio, Reynolds Number and diffusion coefficient on the mixing performance of microchannel and staggered arrangements is

✉ Sandeep Sitaram Wangikar
   sswangikar@coe.sveri.ac.in; sandeep.wangikar@gmail.com

1 Department of Mechanical Engineering, National Institute of Technology Silchar, Silchar, Assam 788010, India

2 Department of Mechanical Engineering, SVERI's College of Engineering, Pandharpur, Maharashtra 413304, India

more suitable for micromixer. The studies of different geometries for the microchannels have been reported by various researchers like rectangular microchannels (Song et al. 2012), T mixer (Wong et al. 2004), 3-D T-mixer (Cortes-Quiroz et al. 2014), sinusoidal convergent–divergent cross-section (Parsa et al. 2014), serpentine microchannels (Das et al. 2017), passive micromixer with circular and square chambers (Gidde et al. 2017), rhombic micromixer (Chung et al. 2010), serpentine microchannel with non-aligned input (Hossain and Kim 2015) etc. The enhanced mixing characteristics have been reported due to the change in geometries leading to chaotic advection. The new designs of microfluidic junctions have been proposed by Sarkar et al. (2014) for better mixing characteristics. The comparative study of various channel geometries like curved, square wave T loop, mouth and zigzag have been performed (Hossain et al. 2009; Kuo and Jiang 2014; Kuo et al. 2016; Chen et al. 2016) for the flow characteristics analysis of microchannels and recommended the square wave microchannel for better mixing performance.

The effects of roughness, fractal dimension, and Reynolds number on mixing in a hexagonal passive micromixer has been studied by Pendharkar et al. (2013) and reported the significance of surface roughness for superior mixing efficiency. The obstructions in the microchannels have been used by some researchers like J-shaped baffles (Lin et al. 2007), baffles with different heights (Chung et al. 2008), diamond shaped obstructions (Asgar et al. 2007, 2008), different shaped obstacles (Sarma and Patowari 2016a, b) and reported that good mixing performance even at lower Reynolds number. Tsai and Wu (2012) have reported the mixing performance analysis of three-stream curved-straight-curved (CSC) micromixers and reported that the full three stream CSC micromixer is the preferable amongst the different configurations considered.

All the above cited works of different researchers demonstrate the achievement of significant improvement in the mixing characteristics by changing the shape of the microchannel and also by using obstacles in the microchannels. In micro-applications like Lab-on-chips, the serpentine microchannels may further reduce the size of the device. Although a number of numerical investigations are reported by different researchers as per the available literature on mixing behavior of serpentine microchannel using different types of obstacles, but comparative assessments on numerical and experimental investigations in this regard are very limited. Thus, studies on the effect of obstacles size on the mixing performance and prediction of obstacle shape and optimum dimensions of obstacle size for a typical microchannel will definitely contribute toward development in this field. Also the scientific explanation for mixing behavior in microchannels for varying the

Reynolds number (Re) is not well established and therefore further investigations are needed.

In this article, the performance characteristics of a simple serpentine microchannel (without obstacles) and microchannel with semicircular obstacles obtained through numerical and experimental investigations have been presented. Numerical models for both the microchannel configurations are developed and their performance characteristics are evaluated. Then both the microchannels have been fabricated and experiments are conducted to evaluate their performance characteristics. The numerical results are validated with the experimental results. Furthermore, the flow physics study has been carried out numerically for analyzing the effect of Re on the mixing index.

2 Methodology

This work has been carried out in three phases. In first phase, the computational models for a simple serpentine microchannel and serpentine microchannels with four different sizes of semicircular obstacles have been developed. Simulations of these models are then carried out for obtaining the pressure drops and mixing lengths. Based on critical analysis of the simulated results, the most suitable semicircular obstacle size for the serpentine microchannels is finalized. In the second phase, a serpentine microchannel with semicircular obstacle along with a simple serpentine microchannel have been fabricated with the same design dimension as that of the computational model. The experiments are then conducted on an experimental setup developed for evaluating pressure drops and mixing indices at different flow conditions. The computational model is then validated with experimental results. Finally in the last phase, the computational analysis has been carried out to study the flow physics in the microchannels using the validated computational model.

2.1 Development of computational model

2.1.1 Microchannel design

The geometries considered for the simple serpentine microchannel and serpentine microchannel with semicircular obstacles with Y shaped inlet have been presented in Fig. 1a, b, respectively. The width and height of the microchannel have been taken same as 380 μm. The five semi circular obstacles have been placed in the serpentine microchannel along the length in each segment with equal adjacent spacing between two obstacles as 1.746 mm. The length of Y inlet is 3 mm and after that a straight segment of length 2 mm connecting to the next segment of

Fig. 1 **a** Simple serpentine microchannel. **b** Serpentine microchannel with semi circular obstacles. **c** Semicircular obstacles with different radii
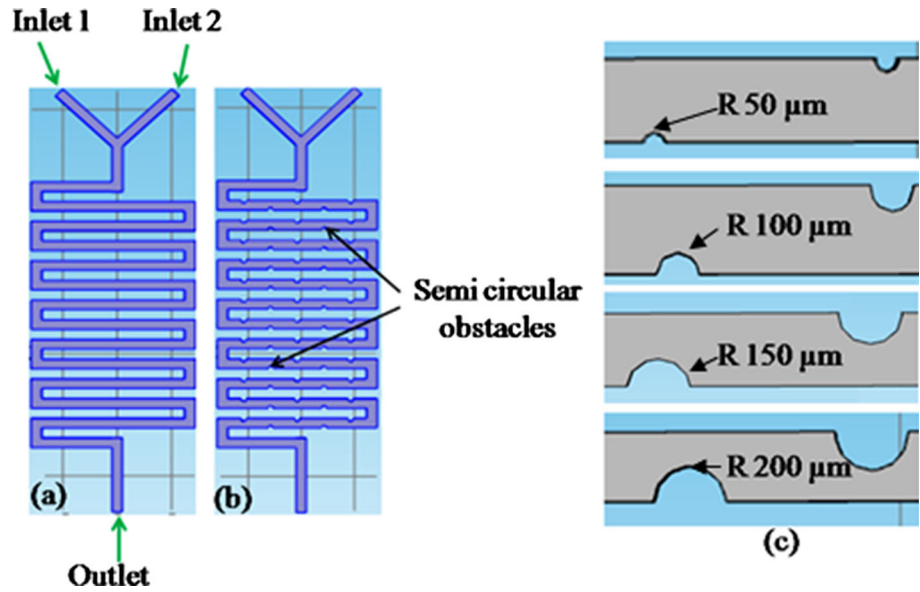
serpentine shape. The total length of the mixing channel is 87.2 mm. Four different cases with semicircular obstacles in the serpentine microchannels having radius as 50, 100, 150, and 200 μm as shown in Fig. 1c have been considered. Two different fluids have been fed through Inlet 1 and Inlet 2. The velocity of both the fluids (mm/s) has been assumed to be equal.

2.1.2 Governing equations

The steady state condition for the flow of fluid and convection and diffusion of the species have been considered in the model. The mass and momentum balances for isothermal, incompressible flow of Newtonian fluids in microchannels are governed by continuity and Navier–Stokes equations. From the scaling analysis, it can be shown that the magnitude of body force term appearing in the momentum equations for the present problem as outlined above are negligibly small as compared to the forces due to advection and diffusion. Accordingly, the components of volume force are not considered in the analysis. The mass and momentum balance equations used in the numerical model are

$$\nabla . \vec{v} = 0 \tag{1}$$

$$\rho(\vec{v} \cdot \nabla)\vec{v} = -\nabla p + \mu \nabla^2 \vec{v}, \tag{2}$$

where ρ is the density of fluid, $\vec{v}$ is the velocity vector, p represents fluid pressure, and μ represents dynamic viscosity of fluid.

The mixing in microchannels has been occurring because of the convection and diffusion. The mass transport has been governed by the following equation:

$$\nabla . (-D_i . \nabla c_i) + u . \nabla c_i = R_i, \tag{3}$$

where, D_i is diffusion coefficient, c_i is concentration of the species, and R_i represents the reaction rate (for diffusive mixing, it is zero).

A Reynolds number (Re) is given by Eq. (4). The Re has been set in the range from 0.28 to 30.

$$Re = \frac{\rho u D_h}{\mu}, \tag{4}$$

where D_h is the hydraulic diameter of the microchannel.

For studying the mixing behavior in microchannels, the mixing index is required to be calculated along the length at different cross sections. The mixing index of the species at any cross section in microchannel is calculated using following equation (Chen et al. 2016):

$$M = 1 - \sqrt{\frac{1}{N} \sum_{i=1}^{N} \left(\frac{C_i - \bar{C}}{\bar{C}} \right)^2}, \tag{5}$$

where, M is the mixing index, N is total number of grid points, C_i is the normalized concentration at any cross section and $\bar{C}$ is the average normalized concentration of the domain. Mixing index ranges from 0 to 1 ($M = 0$ for no mixing and $M = 1$ for 100% mixing).

2.1.3 Boundary conditions

The simple serpentine microchannel and serpentine microchannel with semicircular obstacles as shown in Fig. 1a, b have been designed in COMSOL Multiphysics 5 and simulations have been carried out. Laminar flow and transport of diluted species are selected in COMSOL for simulation. Equations (1)–(3) have been solved by using the appropriate boundary conditions. The same velocities at the two inlets have been employed as boundary conditions.

The inlet velocity is varied from 1 to 144 mm/s. At outlet, atmospheric pressure boundary condition has been used. No slip boundary conditions at the microchannel walls and symmetry boundary conditions have been used at the interface between the fluids. Water and water-$KMnO_4$ at 25 °C have been considered as fluid 1 for first inlet and fluid 2 for the other inlet, respectively. The concentrations of fluids 1 and 2 at the inlet boundaries are kept at 0 and 0.63278 mol/m^3, respectively. The diffusion coefficient of water-$KMnO_4$ is taken as 4.0×10^{-9} m^2/s.

2.1.4 Mesh independence test

The unstructured mesh has been used for the analysis of the microchannel model. Simulations have been carried out with different mesh size (domain elements) to avoid the enhancement of elements in meshing and its effect on the quality of computational results. The mixing index is governed by difference in concentration. The results for pressure drop and difference in concentration has been compared for different domain elements for both the configurations of microchannels. Figure 2a, b show the grid independence tests for the pressure drop, while Fig. 3a, b represents the grid independence test for the difference in concentration for simple serpentine microchannel and serpentine microchannel with semicircular obstacles, respectively.

It has been observed that the results for pressure drop and difference in concentration are observed independent beyond 118,517 and 235,694 domain elements for simple serpentine microchannel and serpentine microchannel with semicircular obstacles as depicted in Figs. 2a, b, 3a, b. Therefore, the domains containing 276,922 elements for simple serpentine microchannel and 347,222 that for serpentine microchannel without obstacles have been found sufficient to predict the mixing characteristics of the microchannel.
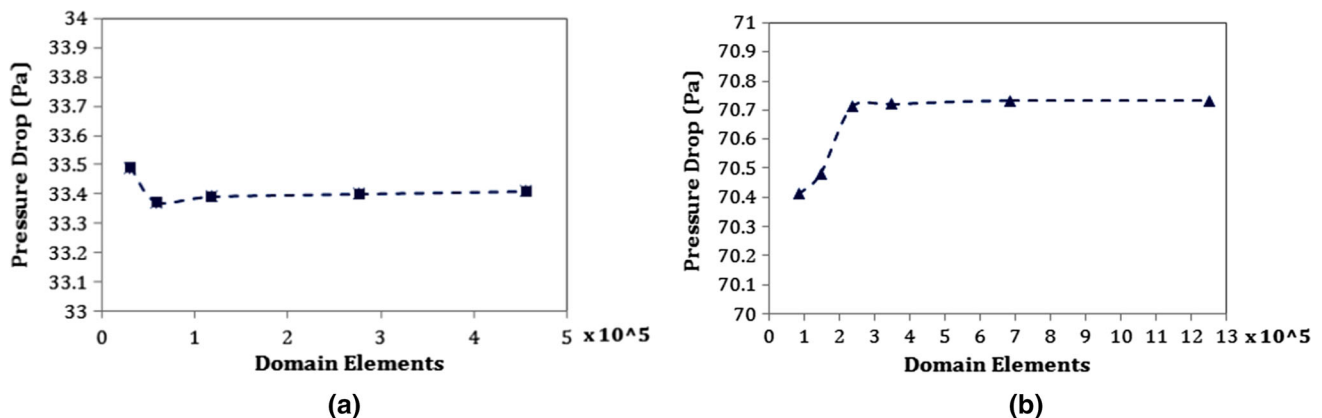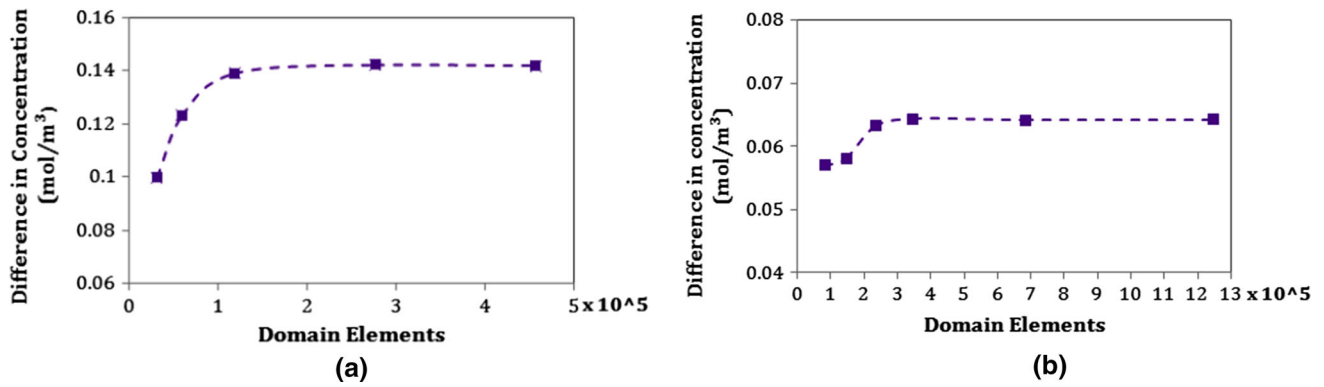
2.1.5 Validation of computational model

The proposed computational model has been validated by comparing the simulation results reported by Das et al. (2017) for serpentine microchannel with Y shaped inlet. The comparison for the difference in concentration results is demonstrated in Fig. 4. The simulation results predicted by the computational model of the present study are in good agreement with that predicted by Das et al. (2017). Therefore, the present computation model is carried forward for further analysis.

2.2 Experimentation

2.2.1 Fabrication of microchannels

The soft lithography process has been employed for fabrication of serpentine microchannels. The master mold has been generated using photochemical machining (PCM) (Wangikar et al. 2017, 2018a, b). The photo tool has been prepared and transferred on a transparent film using offset printing. The PCM has been used to fabricate the brass master molds for simple serpentine microchannel and serpentine microchannel with 150 μm radius semicircular obstacle from material. After that the polydimethylsiloxane (PDMS) solution has been prepared by mixing the base material and curing agent at 10:1 (Sylgard 184), and then the solution is kept in a vacuum desiccator to remove the trapped air bubbles. The PDMS is then poured on the mold to achieve approximate 3 mm thickness. It is then cured on a leveled hotplate for approximately 2.5 h at 80 °C (Asgar et al. 2007). The PDMS is then cut and peeled off cautiously from the master mold of brass. The fabricated PDMS simple serpentine microchannel and serpentine microchannel with 150 μm radius semicircular obstacle are shown in Fig. 5a, c and their magnified views are depicted in Fig. 5b, d, respectively. The scanning electron

Fig. 2 Grid independence test for pressure drop. a Simple serpentine microchannel. b Serpentine microchannel with semicircular obstacles

Fig. 3 Grid independence test for difference in concentration. **a** Simple serpentine microchannel. **b** Serpentine microchannel with semicircular obstacles
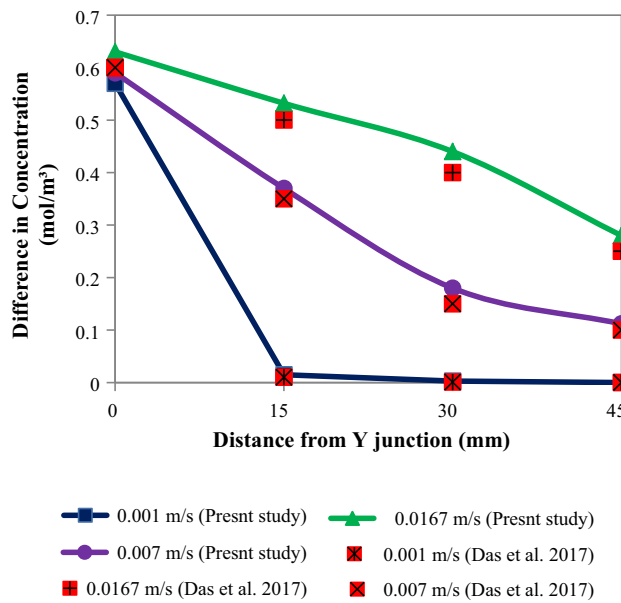
Fig. 4 Validation of computational model for results of concentration (with Das et al. 2017)

microscopy (SEM) images of semicircular obstacle are illustrated in Fig. 5e, f. Using the biopsy punches, the outlet and inlet holes are made in PDMS microchannels from reverse face of a fabricated microchannels. The fabricated PDMS microchannel is then bonded with another similarly fabricated PDMS layer for sealing and testing purpose.

2.2.2 Experimental procedure

The experimental setup has been developed for the intended experimentation with the fabricated serpentine PDMS microchannels and is shown in Fig. 6. The properties of the two considered fluids are shown in Table 1. The twin syringe pump (Make: Yashtech India) has been used for feeding the fluids to the inlets at required velocities. Micro

connectors are used to connect the tubings to the PDMS microchannel. The images for quantifying mixing in the microchannel are captured with Rapid I Vision 5 microscope. The intensity of color of fluid changes as it progresses through the microchannel. Therefore, the images are taken at various locations along the lengths of the serpentine microchannel. The pressure sensor with data logger is incorporated for measurement the pressure drop. The experiments are conducted on the developed experimental setup to evaluate the pressure drops and mixing behavior through the fabricated serpentine PDMS microchannels.

### 2.2.3 Method for quantification of mixing index

The mixing index has been quantified by using statistical approach. The level of mixing within the microchannel can be assessed by the homogeneity and even appropriation of the intensity values of the pixels of an image. A code has been developed for determination of mixing index. At first, the captured RGB image has been converted to a grey scale image. At the grey scale level, 0 represents black and 255 represents white. At the inlet of the microchannel, both the fluids are in unmixed condition and colors of both appears—dark purple for $KMnO_4$-water solution and colorless for water. At this stage, the average pixel intensity of the image is approximately 130. This is treated as 0% mixing (i.e. M = 0). Again at fully mixed stage, the color is mostly blackish on grey scale having average pixel intensity below 10 and this is considered as 100% mixing (M = 1). Based on this, different images have been captured at different mixing lengths in the direction of flow through microchannel to analyze their mixing index.

2.3 Flow physics study

The results obtained from computational model for different flow conditions are validated with the experimental
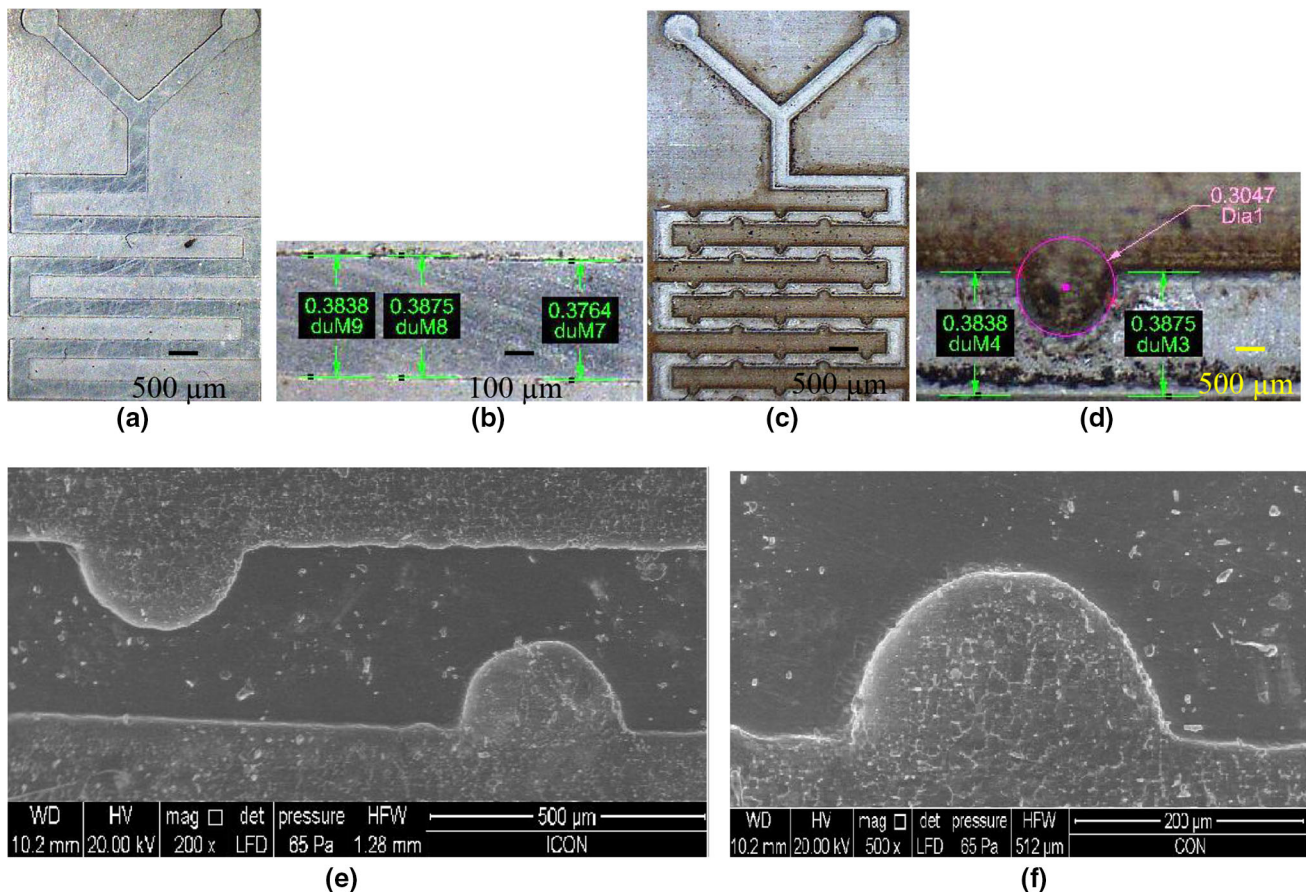
Fig. 5 a PDMS simple serpentine microchannel. **b** Magnified view of simple serpentine microchannel. **c** PDMS serpentine microchannel with 150 μm radius semicircular obstacle. **d** Magnified view of semicircular obstacle. **e**, **f** SEM images of semicircular obstacles
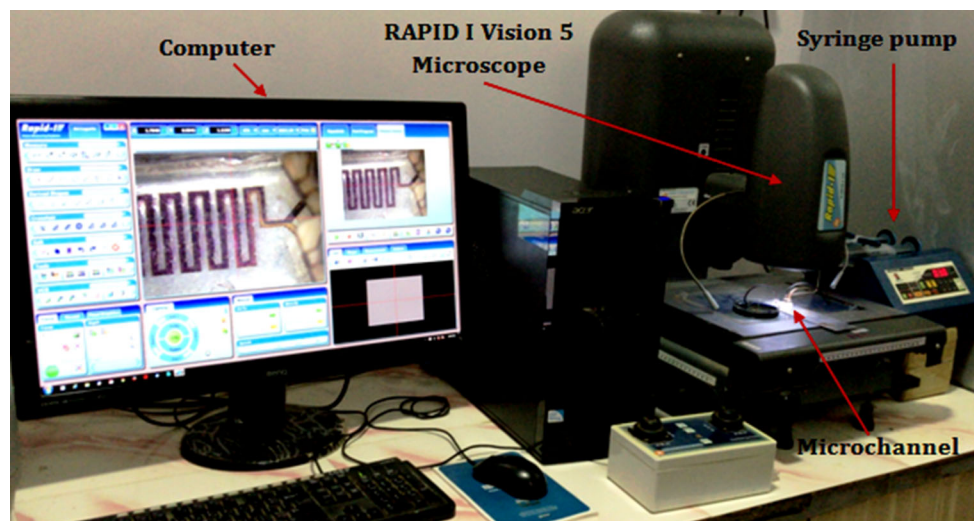
Fig. 6 Experimental set up for micro mixing in microchannels

results. The computational analysis is then extended with the same computational model in order to study the effect of increasing Re on flow characteristics and mixing length in serpentine microchannel with obstacles. At lower Re

flow is laminar and the mixing is due to diffusion only. As Re increases, the effect of secondary flows plays a noteworthy role in mixing characteristics within microchannel. To evaluate the mixing characteristics with increasing Re,

Table 1 Properties of considered fluids

Fluids	Viscosity (Pa s)	Diffusion coefficient (m²/s)	Density (kg/m³)	Concentration (mol/m³)
Water	0.001	1×10^{-9}	1000	0
Water-KMnO$_4$	0.00126	4×10^{-9}	1020	0.63278

the computational analysis has been carried out for Re = 0.28, 5, 10, 15, 20, 25, and 30 through a study on the flow physics in these cases.

# 3 Results and discussion

3.1 Computational analysis

The 3D models of the simple serpentine microchannel and serpentine microchannels with semicircular obstacles have been developed in COMSOL Multiphysics software and simulations have been carried out. Using appropriate boundary conditions, the governing Eqs. (1)–(3) have been solved. Water and KMnO$_4$-water at 25 °C have been used as the primary and secondary fluids respectively.

3.1.1 Effect of obstacle size

The size of semicircular obstacles in serpentine microchannels has been varied by considering the radius as 50, 100, 150, and 200 μm (refer Fig. 1c) to study the effect on the mixing performance of the microchannels. The performance is generally governed by the mixing length and consequently the mixing index. The pressure drop also greatly influences the performance of the microchannels. Thus, the pressure drops and mixing lengths for achieving

mixing index 1 (i.e. 100% mixing) for serpentine microchannels with various obstacle sizes against increasing Re have been evaluated through simulations and illustrated in Fig. 7a, b, respectively.

It has been observed that the pressure drop increases with an increase in Re. The pressure drop has been found to be the highest for a serpentine microchannel with 200 μm obstacle and the least for a microchannel without obstacles. The obstacles in the microchannels are creating restrictions along the flow. This causes the increase in pressure drop with increase in the obstacle size. Hence, higher pressure drop has been observed for semicircular obstacle with radius 200 μm and is gradually decreased from 200 to 50 μm radius obstacles. The mixing length has been observed least for serpentine microchannel with 200 μm radius and highest for simple serpentine microchannel i.e. without obstacles. The minimum mixing length is observed at Re 0.28 as the mixing is due to diffusion only. Further, as Re increases from 0.28 to 10, the mixing length is found to be increasing for all configurations of microchannels. For this range, the fluid is getting lesser time for diffusion and also there is no significant advection and growth of secondary flows. Then, with further increase in Re from 10 to 30, the mixing length gradually decreases. In this increasing span of Re, advection takes place in the direction of flow and thereby secondary flows are generated for the serpentine microchannel with semicircular obstacles.
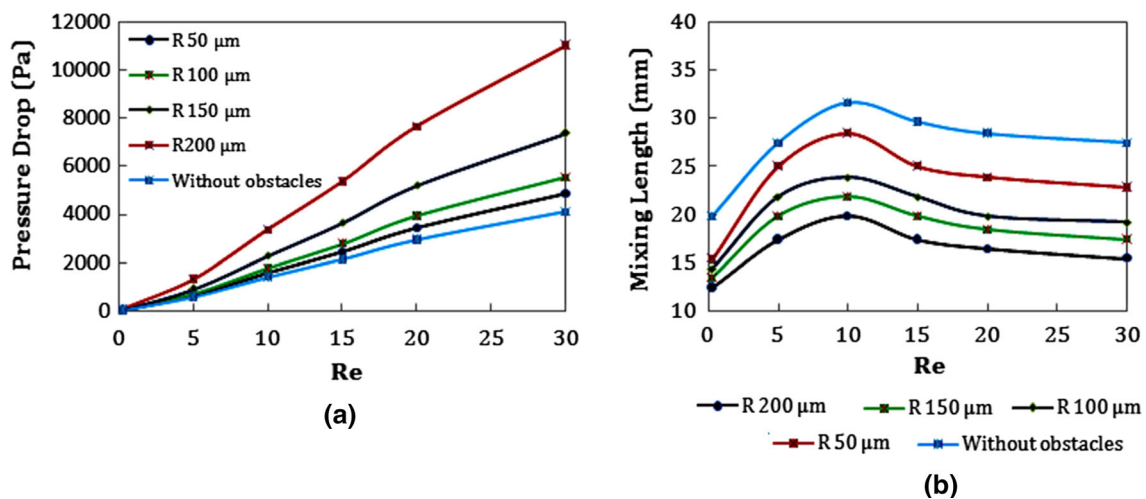

Fig. 7 Effect of Re for serpentine microchannels on **a** pressure drop, **b** mixing length
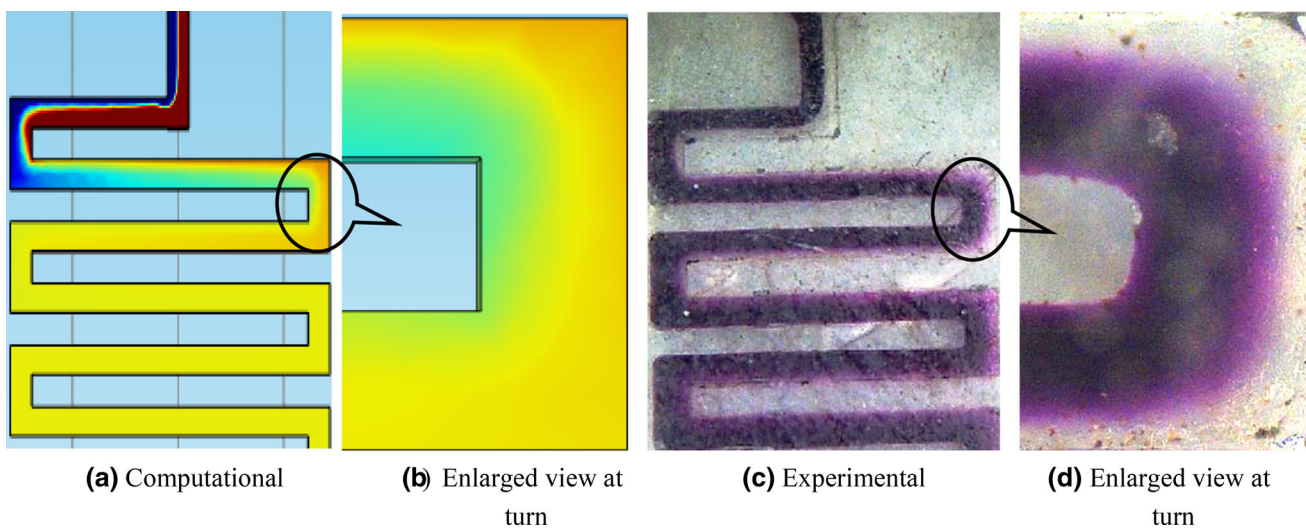
3.2 Experimental analysis

The mixing behavior study has been performed by analyzing the images captured at different locations for a simple serpentine microchannel and a serpentine microchannel with 150 μm radius semicircular obstacles. Figures 8 and 9 demonstrates the comparative mixing behavior analysis based on computational and experimental images at Re 0.28 and Re 15, respectively. The flow is laminar at lower Re (Re = 0.28) and the mixing in the microchannels happens due to diffusion. Therefore it is observed that mixing at Re 0.28 (Fig. 8a, c) occurs in shorter length as compared to that for Re 15 (Fig. 9a, c). The mixing at the entrance after Y junction (enlarged view)

is depicted in Fig. 8b, d and the enlarged view of the turn in a serpentine microchannel is presented in Fig. 9b, d from computational model and experimentation.

The mixing behavior analysis based on computational model and experimentation for a serpentine microchannel with 150 μm radius semicircular obstacles is demonstrated in Fig. 10. The mixing images at Re 0.28 and Re 15 are shown in Fig. 10a, b and Fig. 10c, d respectively. For Re 0.28, at the interface between the two fluids, a diffusive mixing layer has been developed as shown in Fig. 10e, f through simulation model and during experimentation, respectively. These images clearly depict that mixing gets intensified as the flow encounters obstacle in the direction of flow.

(a) Computational   **(b)** Enlarged view at entrance   **(c)** Experimental   **(d)** Enlarged view at entrance
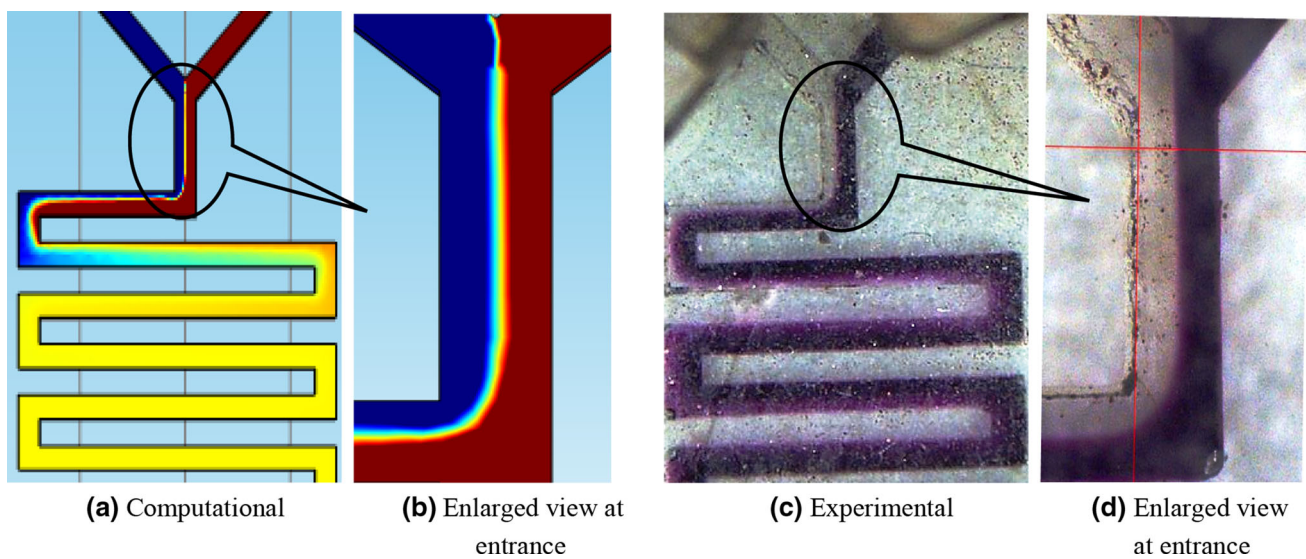
Fig. 8 Mixing images for a simple serpentine microchannel at Re = 0.28

(a) Computational   **(b)** Enlarged view at turn   **(c)** Experimental   **(d)** Enlarged view at turn

Fig. 9 Mixing images for a simple serpentine microchannel at Re = 15

Re 0.28

(a) Computational   **(b)** Experimental

Re 15

(c) Computational   **(d)** Experimental

Enlarged view at turn for Re 0.28

(e) Computational   **(f)** Experimental

Enlarged view at turn for Re 15

(g) Computational   **(h)** Experimental

(i) Computational

(j) Experimental

Enlarged view along the length of microchannel
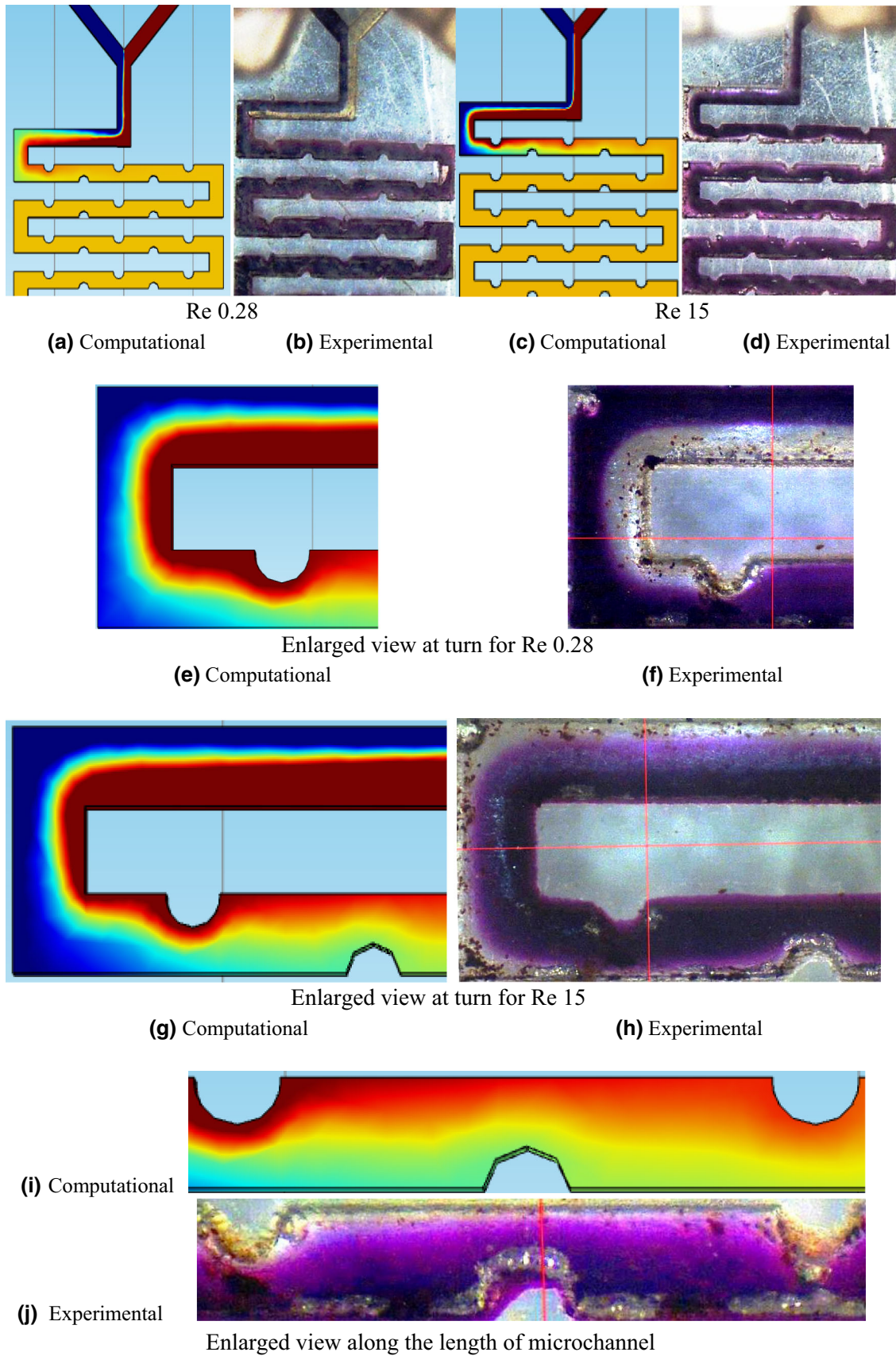
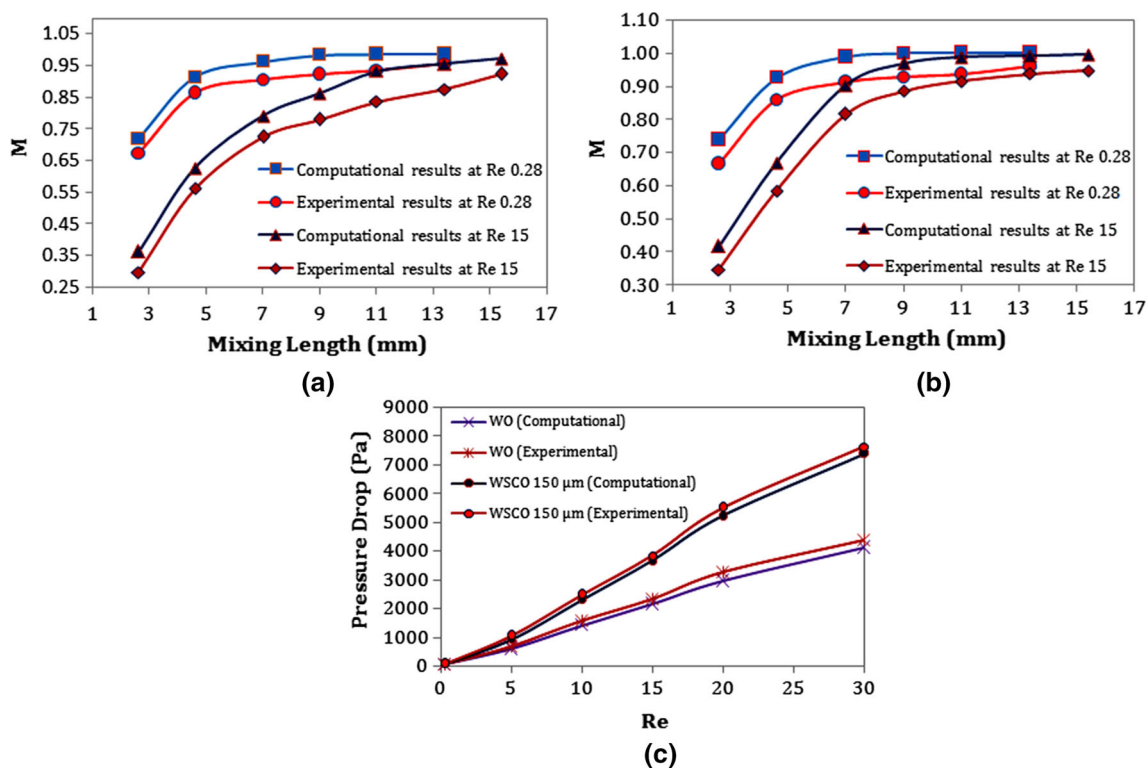**Fig. 10** Mixing images for a serpentine microchannel with 150 μm radius semicircular obstacles

Advection has been induced in the fluid due to the obstacles, resulting in better penetration of fluids into one another and consequently improves mixing as shown in Fig. 10g, h obtained from the computational model and experimentation, respectively. Figure 10i, j depicts enlarged views along the length of microchannel using computational model and experimentation, which reveal the effect of obstacles in the direction flow leading to the advection.

The mixing index for all the fabricated serpentine microchannels have been experimentally evaluated by capturing images at different prefixed mixing lengths in the direction of flow and using developed code for the intended purpose. The same mixing indices are also generated from the computational model using Eq. (5). The experimentally obtained mixing indices are compared with those generated from computational model at Re 0.28 and 15 for simple serpentine microchannel and serpentine microchannels with semicircular obstacles 150 μm radius and are depicted in Fig. 11a, b, respectively. The pressure drop has been recorded experimentally for simple serpentine microchannel and serpentine microchannel with semicircular obstacles with radius of 150 μm, at six different Re ranging from 0.28 to 30. The variation in pressure drop against Re is presented in Fig. 11c. It is observed that the pressure drop increases with

increase in the Re. The pressure drop for microchannel with obstacles is observed higher than that for a simple microchannel. This is due to the obstacles, creating restrictions along the direction of flow leads to increased pressure drop. The experimental results for pressure drop and mixing index for simple serpentine microchannel and serpentine microchannel with semicircular obstacles with radius of 150 μm are found to be in good agreement with the computational results. Thus, the computational model is validated and can be used for further flow physics study.

3.3 Flow physics study

In flow physics study, the mixing characteristics have been analyzed considering the mixing index. The analysis for mixing index has been performed for a simple serpentine microchannel and serpentine microchannel with semicircular obstacles. The mixing index is calculated using Eq. (5) based on the simulation results for different Re. The mixing index for increasing mixing length (ML) for the simple serpentine microchannel and serpentine microchannel with semicircular obstacles at different Re is shown in Fig. 12. The flow patterns developed along the direction of flow near the obstacles for different Re is demonstrated in Fig. 13.

Fig. 11 Validation of computational results with experimental results for **a** mixing index for simple serpentine microchannel, **b** mixing index for serpentine microchannel with 150 μm radius semicircular obstacles, and **c** pressure drop for simple serpentine microchannel (without obstacles—WO) and for serpentine microchannel with 150 μm radius semicircular obstacles (WSCO 150 μm)
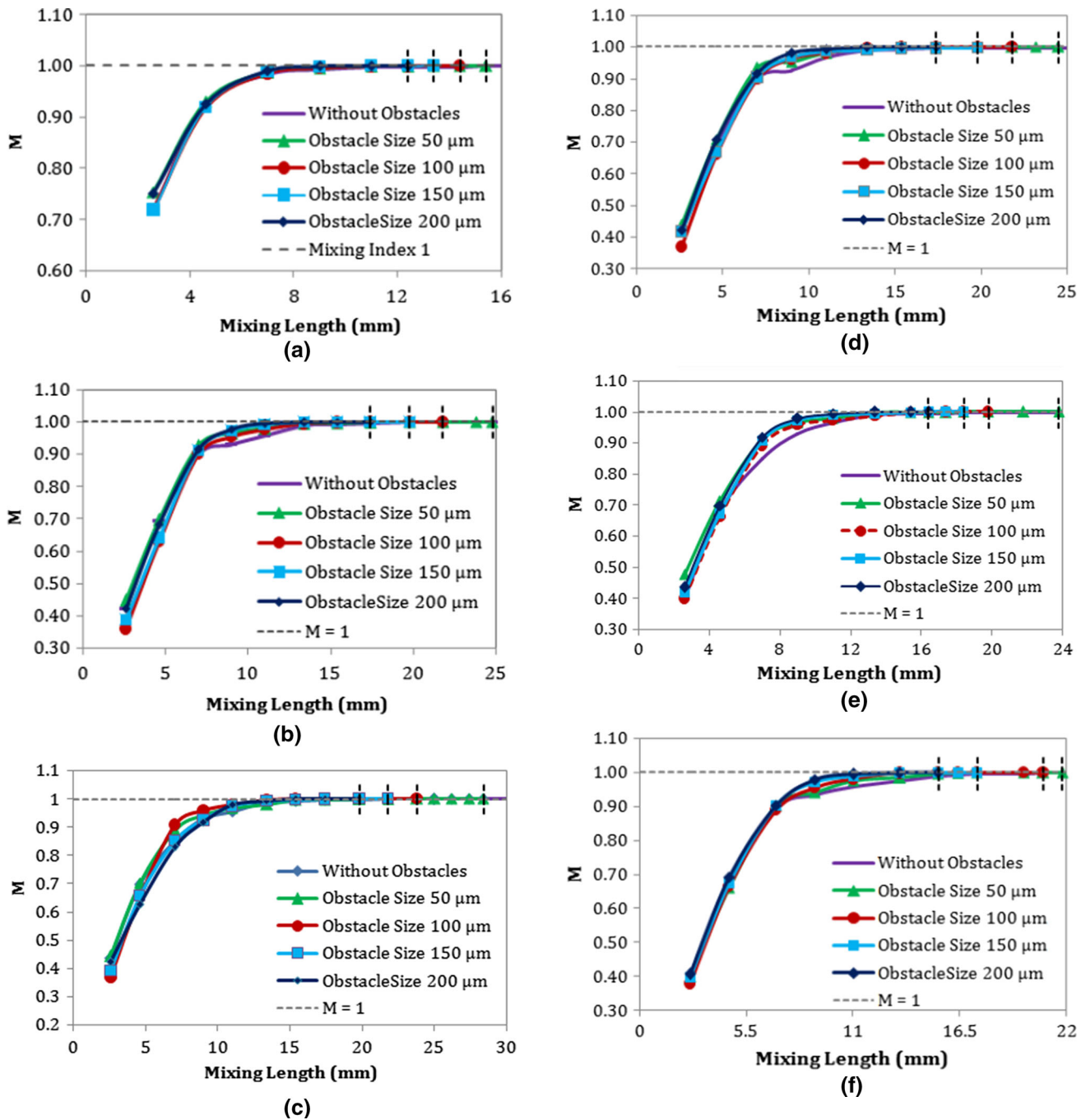
Fig. 12 Mixing Index along mixing lengths for **a** Re = 0.28, **b** Re = 5, **c** Re = 10, **d** Re = 15, **e** Re = 20, and **f** Re = 30

Fig. 12 continued

The 100% mixing is represented as mixing index 1 (i.e. M = 1). Figure 12a shows the mixing index performance of the microchannels at Re = 0.28. The mixing index 1 is achieved for simple serpentine microchannel in 19.8 mm ML, while that for the serpentine microchannel with semicircular obstacles is achieved in 12.4, 13.4, 14.4 and 15.4 mm for obstacles with radius 50, 100, 150, and 200 μm, respectively, which are shown by dotted line in

Fig. 12a. At Re 0.28, the mixing is due to diffusion only. Also at Re 0.28, due to very less velocity, no secondary flows or vortices are generated near the obstacle in the flow as depicted in Fig. 13a.

Increase in Re is due to increased velocities of the fluids. With increase in Re up to 5 and further up to 10, the time for diffusion of fluids is getting reduced and at these velocities, no advection and thus no secondary flows are developed. Thus, increased MLs have been observed for attaining mixing index 1 at Re 5 and Re 10 for all the

Fig. 13 Flow patterns along the direction of flow at various Re for serpentine microchannel with obstacles
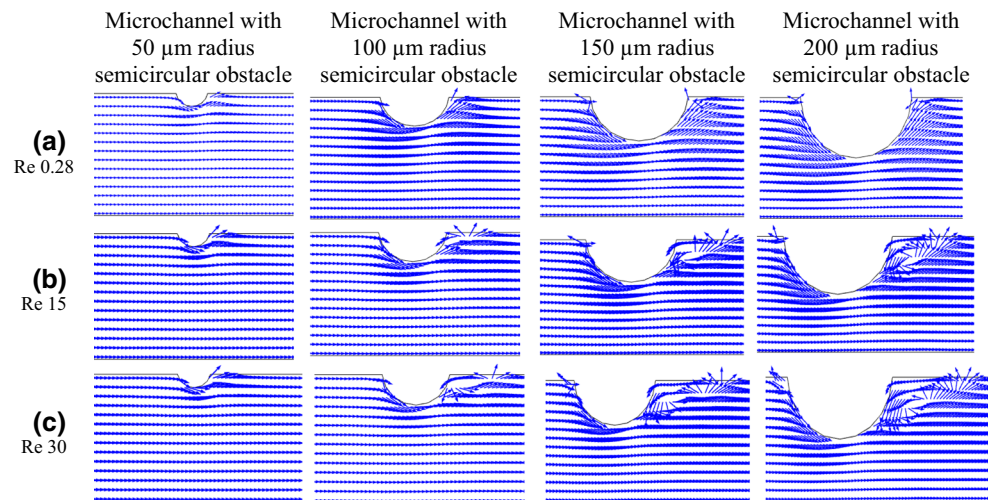
Fig. 14 Vortices generation near the obstacles (computational and experimental) at various Re for serpentine microchannel with 150 μm radius obstacles
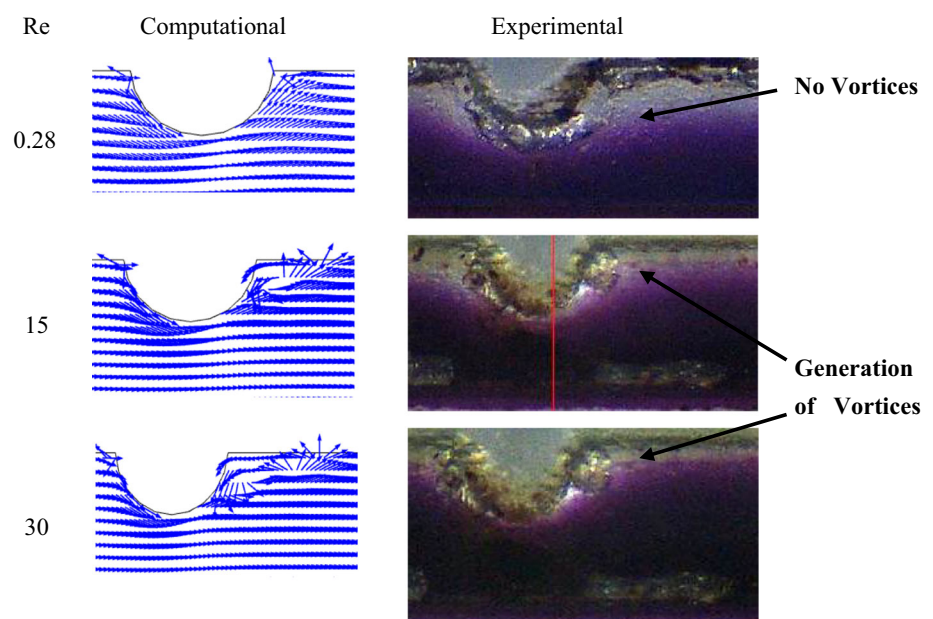
configurations of serpentine microchannels as shown in Fig. 12b, c respectively.

The fluid at the inside corner accelerates while fluid at the outside corner decelerates when the fluid experiences turning. The degree of acceleration is depends upon to the degree of turning (the reciprocal of the radius of rotation), variation of the cross section, and the flow velocity (Yang and Lin 2006; Gidde et al. 2017). As well, the degree of acceleration decides the strength and scale of the induced vortex which deforms and enhances an interface between the fluids. The fluid at the inner corner represses the outer corner fluid and then flows back along the wall. Two fluids thereby become agitated. This agitation of circulation is advances with increase in Re and consequently, the interfacial area of fluids gets distorted and increased. Taken as a whole, the positive outcome of growing the flow velocity in

fluid mixing is the amplified interfacial area, while the negative influence is the decreased period of residence. The generation of vortices at the turn in the serpentine channels play a significant role in mixing for all considered five cases of serpentine microchannels, especially for microchannel without obstacles. This vortices generation may takes place from Re 15 to 30, due to which enhancement in mixing with decreasing mixing lengths are observed.

However, at Re = 15, the development of secondary flows (vortices generation) starts for serpentine microchannel with 100 μm radius obstacle and these are found to be higher with increase in obstacle sizes (150 and 200 μm) as clearly visible in Fig. 13b. This leads to enhanced mixing results in comparatively shorter ML for achieving mixing index 1, as depicted in Fig. 12d. This

trend continues for Re 20 and due to increased advection and secondary flows, further decreased MLs are observed for all configurations of microchannels, as shown in Fig. 12e.

The mixing index achieved for different MLs at Re 30 has been presented in Fig. 12f. The secondary flows developed along the flow direction near the obstacles is shown in Fig. 12c. The intensity of vortices generated for serpentine microchannel with 100, 150 and 200 μm radius obstacle is more (Fig. 13c) as compared to previous cases and continues to be increasing. This leads improved mixing characteristics and reduced ML for serpentine microchannel with 200 μm radius semicircular obstacles.

In case of microchannels with obstacles, the growth in the mixing layer along the direction of flow is much better and accordingly uniform mixing has been observed in less mixing length. Figure 14 shows the images for vortices generation in serpentine microchannel with 150 μm radius obtained through experimentation which complement the computational images. As the size of semicircular obstacles increases from radius 50 μm to radius 200 μm, advection has also been increasing along with generation of secondary flows resulting in better growth in the mixing layer along the direction of flow and in turn better mixing is observed in shorter MLs. Thus, ML in serpentine microchannels is observed to be least for 200 μm radius semicircular obstacle, followed by 150 and 100 μm radius semicircular obstacle and is the higher for 50 μm radius semicircular obstacle for all the considered Re. For all serpentine microchannels with semicircular obstacles, MLs required to achieve mixing index 1 are observed to be lesser in comparison to that for simple serpentine microchannels. This is due to advection and secondary flows developed near the obstacles as shown in Fig. 13.

4 Conclusions

The mixing performance of a simple serpentine microchannel and serpentine microchannel with semicircular obstacles having radius 150 μm has been studied using computational analysis with COMSOL Multiphysics software and experimental analysis. Further in the computational analysis, the semicircular obstacles size has been varied by considering the radius as 50, 100, 150, and 200 μm. The pressure drop is observed to be lesser for a simple serpentine microchannel and then for serpentine microchannel with 50 μm radius obstacle microchannel and the lower mixing length for attaining mixing index 1 is obtained with 200 μm obstacle in serpentine microchannel. The experiments are conducted by fabricating a simple serpentine microchannel and a serpentine microchannel with 150 μm semicircular obstacles. The mixing index and

pressure drop analysis has been performed at Re = 0.28, 5, 10, 15, 20, and 30 and a good agreement has been observed between the computational and experimental results. The pressure drop for both the configurations is seen increasing with increase in the Re. The mixing lengths are observed to be lesser for Re = 0.28 and 30 and higher for Re = 10 for all the configurations of considered serpentine microchannels. The flow physics study clearly demonstrates the effect of diffusion at lower Re and generation of secondary flows due to advection at higher Re. Thus, this study justifies obtained results through experimentation as well as computational models.

References

Asgar A, Bhagat S, Peterson ETK, Papautsky I (2007) A passive planar micromixer with obstructions for mixing at low Reynolds numbers. J Micromech Microeng 17:1017–1024. https://doi.org/10.1088/0960-1317/17/5/023

Asgar A, Bhagat S, Papautsky I (2008) Enhancing particle dispersion in a passive planar micromixer using rectangular obstacles. J Micromech Microeng 18:85005. https://doi.org/10.1088/0960-1317/18/8/085005

Capretto L, Cheng W, Hill M, Zhang X (2011) Micromixing within microfluidic devices. Top Curr Chem 304:27–68. https://doi.org/10.1007/128_2011_150

Chen X, Li T, Hu Z (2016) A novel research on serpentine microchannels of passive micromixers. Microsyst Technol. https://doi.org/10.1007/s00542-016-3060-7

Chung CK, Wu CY, Shih TR (2008) Effect of baffle height and Reynolds number on fluid mixing. Microsyst Technol 14:1317–1323. https://doi.org/10.1007/s00542-007-0511-1

Chung CK, Shih TR, Wu BH, Chang CK (2010) Design and mixing efficiency of rhombic micromixer with flat angles. Microsyst Technol 16:1594–1600. https://doi.org/10.1007/s00542-009-0980-5

Cortes-Quiroz CA, Azarbadegan A, Zangeneh M (2014) Evaluation of flow characteristics that give higher mixing performance in the 3-D T-mixer versus the typical T-mixer. Sens Actuators B 202:1209–1219. https://doi.org/10.1016/j.snb.2014.06.042

Das SS, Tilekar SD, Wangikar SS, Patowari PK (2017) Numerical and experimental study of passive fluids mixing in microchannels of different configurations. Microsyst Technol 23:5977–5988

Gidde RR, Pawar PM, Ronge BP, Misal ND, Kapurkar RB, Parkhe AK (2017) Evaluation of the mixing performance in a planar passive micromixer with circular and square mixing chambers. Microsyst Technol. https://doi.org/10.1007/s00542-017-3686-00123456789 (accepted article)

Hossain S, Kim KY (2015) Mixing performance of a serpentine micromixer with non-aligned inputs. Micromachines 6:842–854. https://doi.org/10.3390/mi6070842

Hossain S, Ansari MA, Kim KY (2009) Evaluation of the mixing performance of three passive micromixers. Chem Eng J 150:492–501. https://doi.org/10.1016/j.cej.2009.02.033

Kuo JN, Jiang LR (2014) Design optimization of micromixer with square-wave microchannel on compact disk microfluidic platform. Microsyst Technol 20:91–99. https://doi.org/10.1007/s00542-013-1769-0

Kuo JN, Liao HS, Li XM (2016) Design optimization of capillary-driven micromixer with square-wave microchannel for blood plasma mixing. Microsyst Technol. https://doi.org/10.1007/s00542-015-2722-1

Lee CY, Wang WT, Liu CC, Fu LM (2016) Passive mixers in microfluidic systems: a review. Chem Eng J 288:146–160. https://doi.org/10.1016/j.cej.2015.10.122

Lim YC, Kouzani AZ, Duan W (2010) Lab-on-a-chip: a component view. Microsyst Technol 16:1995–2015. https://doi.org/10.1007/s00542-010-1141-6

Lin YC, Chung YC, Yu CY (2007) Mixing enhancement of the passive microfluidic mixer with J-shaped baffles in the tee channel. Biomed Microdevices 9:215–221. https://doi.org/10.1007/s10544-006-9023-5

Parsa MK, Hormozi F, Jafari D (2014) Mixing enhancement in a passive micromixer with convergent-divergent sinusoidal microchannels and different ratio of amplitude to wave length. Comput Fluids 105:82–90. https://doi.org/10.1016/j.compfluid.2014.09.024

Pendharkar G, Deshmukh R, Patrikar R (2013) Investigation of surface roughness effects on fluid flow in passive micromixer. Microsyst Technol 20:2261–2269. https://doi.org/10.1007/s00542-013-1957-y

Sahu PK, Golia A, Sen AK (2012) Analytical, numerical and experimental investigations of mixing fluids in microchannel. Microsyst Technol 18:823–832. https://doi.org/10.1007/s00542-012-1511-3

Sahu PK, Golia A, Sen AK (2013) Investigations into mixing of fluids in microchannels with lateral obstructions. Microsyst Technol 19:493–501. https://doi.org/10.1007/s00542-012-1617-7

Sarkar S, Singh KK, Shankar V, Shenoy KT (2014) Numerical simulation of mixing at 1–1 and 1–2 micro fluidic junctions. Chem Eng Process 85:227–240. https://doi.org/10.1016/j.cep.2014.08.010

Sarma P, Patowari PK (2016a) Design and analysis of passive Y-type micromixers for enhanced mixing performance for biomedical and microreactor application. J Adv Manuf Syst 15(03):161–172

Sarma P, Patowari PK (2016b) Study on design modification of serpentine micromixers for better throughput for microfluidic circuitry. Micro Nanosyst 8(2):19–125

Song H, Wang Y, Pant K (2012) Cross-stream diffusion under pressure-driven flow in microchannels with arbitrary aspect ratios: a phase diagram study using a three-dimensional analytical model. Microfluid Nanofluid 12:265–277. https://doi.org/10.1007/s10404-011-0870-x

Tsai RT, Wu CY (2012) Multidirectional vortices mixing in three-stream micromixers with two inlets. Microsyst Technol 18:779–786. https://doi.org/10.1007/s00542-012-1516-y

Wangikar SS, Patowari PK, Misra RD (2017) Effect of process parameters and optimization for photochemical machining of brass and german silver. Mater Manuf Process 32(15):1747–1755. https://doi.org/10.1080/10426914.2016.1244848

Wangikar SS, Patowari PK, Misra RD (2018a) Parametric optimization for photochemical machining of copper using overall evaluation criteria. Mater Today. https://doi.org/10.1016/j.matpr.2017.12.046 **(accepted article)**

Wangikar SS, Patowari PK, Misra RD (2018) Parametric optimization for photochemical machining of copper using grey relational method. Springer International Publishing AG 2018, Techno-Societal 2016. https://doi.org/10.1007/978-3-319-53556-2_94

Wong SH, Ward MCL, Wharton CW (2004) Micro T-mixer as a rapid mixing micromixer. Sens Actuators B 100:359–379. https://doi.org/10.1016/j.snb.2004.02.008

Yang JT, Lin KW (2006) Mixing and separation of two-fluid flow in a micro planar serpentine channel. J Micromech Microeng 16(11):2439